

A High-Resolution Survey of a Deep Hydrocarbon Plume in the Gulf of Mexico During the 2010 Macondo Blowout

J. P. Ryan,¹ Y. Zhang,¹ H. Thomas,¹ E. V. Rienecker,¹ R. K. Nelson,² and S. R. Cummings³

Following destruction of the *Deepwater Horizon* drilling rig, while unmitigated blowout from the Macondo well was ongoing, NOAA scientific response cruise GU-10-02 (27 May to 4 June 2010) employed coordinated ship and autonomous underwater vehicle (AUV) operations to locate and study deep hydrocarbon plumes. The ship hydrocast survey localized maximum optical signals of a deep plume, centered at ~1150 m depth, approximately 13 km southwest of the blowout. Deployed at this location, the AUV conducted a high-resolution survey of plume structure, which indicated small-scale topographic influences on plume transport. Maximum plume intensity was observed along the western slope of Biloxi Dome. The orientation of gradients in plume intensity relative to isobaths indicated flow from the dome slope onto the dome top. In terms of the relative proportions of major hydrocarbon groups, all plume samples southwest of the blowout exhibited similar composition. The chemical composition of the plume southwest of the blowout was significantly different from the composition of a weaker deep plume observed southeast of the blowout. Variation in optical signal from a colored dissolved organic matter (CDOM) fluorometer (F_{CDOM}) explained up to 97% (median 88%) of the variance in the concentrations of individual hydrocarbon compounds. AUV data also showed that F_{CDOM} was highly correlated with three other optical measurements ($r > 0.97$) and oxygen measurements ($r = -0.95$). The results provide unique perspective on small-scale dynamics of a deep plume and illustrate the potential for studying subsurface plumes of dispersed oil using AUVs with off-the-shelf sensors.

1. INTRODUCTION

As a massive anthropogenic perturbation entered the Gulf of Mexico following the accidental destruction of the *Deep-*

water Horizon drilling platform above the BP Macondo Prospect well (MC 252 #1) in late April 2010, extensive information was being gathered at the boundaries of the disaster. The bottom boundary was closely monitored throughout prolonged efforts to understand the damaged wellhead structure, quantify flow rates, and stop the blowout. The ocean surface and shoreline boundaries were closely observed from satellites, aircraft, ships, and shore during sustained efforts to understand and predict the transport of oil, remove or disperse the oil, and block its incursion into coastal environments. While urgency drove intensive observation of the Gulf's boundaries, the vast volume of ocean between the boundaries received relatively little attention and effort. However, beginning in mid-May, ship surveys began to reveal that some of the blowout oil was not rising to the surface. Diffuse plumes of oil, dispersed at the wellhead,

¹Monterey Bay Aquarium Research Institute, Moss Landing, California, USA.

²Woods Hole Oceanographic Institution, Woods Hole, Massachusetts, USA.

³NOAA Atlantic Oceanographic and Meteorological Laboratory, Miami, Florida, USA.

were remaining in the deep ocean, with their strongest evidence found southwest of the blowout [Diercks *et al.*, 2010; Joint Analysis Group (JAG), 2010a, 2010b; Hazen *et al.*, 2010]. Despite convincing evidence, the existence of deep plumes became a controversial topic in the complex interactions between scientific research and the legal/political system [Schrope, 2010]. Our research efforts began during late May, in the midst of this controversy. At this time, early efforts to cap the well had failed, oil was not yet being directly recovered from the damaged wellhead structure, and unmitigated pollution from the blowout was near its peak. The purpose of our cruise was to study subsurface oil and thereby help fill the large information gap between the ocean boundaries.

The response of the marine research community to the *Deepwater Horizon* incident included accelerated adaptation of technologies, many of which were not developed specifically for studying oil in the marine environment. One of these adapted technologies was the *Dorado* autonomous underwater vehicle (AUV), which was developed by the Monterey Bay Aquarium Research Institute for coastal marine research. Capabilities of *Dorado* that make it effective for coastal oceanography include fast propulsion (~ 3 kn = 5.6 km h⁻¹) for synoptic surveying of rapidly changing conditions, a multidisciplinary sensor suite for interdisciplinary research, and a water sample acquisition system that targets sampling according to autonomously detected features of interest. These capabilities have been applied to study a variety of complex coastal ocean processes [Johnson and Needoba, 2008; Ryan *et al.*, 2008a, 2008b, 2009, 2010a, 2010b, 2010c], and they were appropriate for meeting the needs of studying dispersed oil plumes in the water column. Another AUV, *Sentry* (Woods Hole Oceanographic Institution), was equipped with an in situ mass spectrometer specifically for the *Deepwater Horizon* response effort [Camilli *et al.*, 2010]. During surveys in late June 2010, consistent with the findings of previous ship surveys, *Sentry* mapped a continuous hydrocarbon plume extending southwest of the blowout for at least 35 km. Its onboard hydrocarbon detection and quantification, combined with its measurements of water velocity, supported definitive confirmation that the apparently persistent plume southwest of MC 252 #1 must have had its source in the blowout. This was an important confirmation because of the potential confusion between anthropogenic signal of the Macondo blowout and natural signal of seafloor hydrocarbon seeps [JAG, 2010b, Figure 46]. With the goal of informing scientific response operations, *Dorado* observations of the plume southwest of the blowout during early June were provided to the *Sentry* team prior to their deployment [Camilli *et al.*, 2010].

Together, ship and AUV surveys revealed a deep hydrocarbon plume extending southwest of the blowout and persisting for months [JAG, 2010a, 2010b; Camilli *et al.*, 2010; Diercks *et al.*, 2010; Hazen *et al.*, 2010]. Deep-plume transport southwestward along the continental slope was indicated by not only in situ observations, but also model studies [Liu *et al.*, 2011, this volume]. Although evidence of deep-plume transport was found in a range of directions around the wellhead [Valentine *et al.*, 2010; Kessler *et al.*, 2011], the largest and most persistent plume was evidently southwest of the blowout [JAG, 2010a, 2010b; Camilli *et al.*, 2010]. After MC 252 #1 was effectively sealed, ship surveys revealed biogeochemical anomalies of the deep plume extending 500 km along the continental slope southwest of the wellhead [Kessler *et al.*, 2011].

In this contribution, we present deep-plume observations acquired between the time of its discovery southwest of the damaged wellhead and the time of its confirmed link to the blowout. We illustrate how ship hydrocast and AUV systems were employed sequentially to localize deep-plume signal, then map plume structure at high resolution to reveal evidence of small-scale topographic influences on plume transport. Next, we examine the chemical composition of the deep plume southwest of the blowout relative to the composition of a weaker deep plume that we observed southeast of the blowout. Finally, we examine how well optical measurements from an off-the-shelf sensor served as a proxy for hydrocarbon concentrations in our plume samples.

2. DATA AND METHODS

2.1. Ship Hydrocast

Scientific response cruise GU-10-02 conducted survey operations from the NOAA Ship *Gordon Gunter* between 28 May and 3 June 2010. The *Gunter* was equipped with a hydrocast-rossette system for acquiring water column profiles of physical, chemical, and optical properties and returning samples (Figure 1a). The hydrocast system was washed with detergent following each station and maintained in a detergent bath between stations. Protocol for ship hydrocast sampling and data management during NOAA scientific response surveys has been summarized [JAG, 2010c]. Hydrocast sensors included a Sea-Bird 9 conductivity, temperature, and depth (CTD) sensor, a Sea-Bird SBE 43 dissolved oxygen sensor, and a WET Labs CD2000 colored dissolved organic matter (CDOM) fluorometer. Although not designed to measure the concentration of oil in seawater, this type of CDOM fluorometer was proven to be highly responsive to mixtures of MC 252 #1 source oil and the Corexit dispersant that was being applied to disperse the oil [JAG, 2010b].

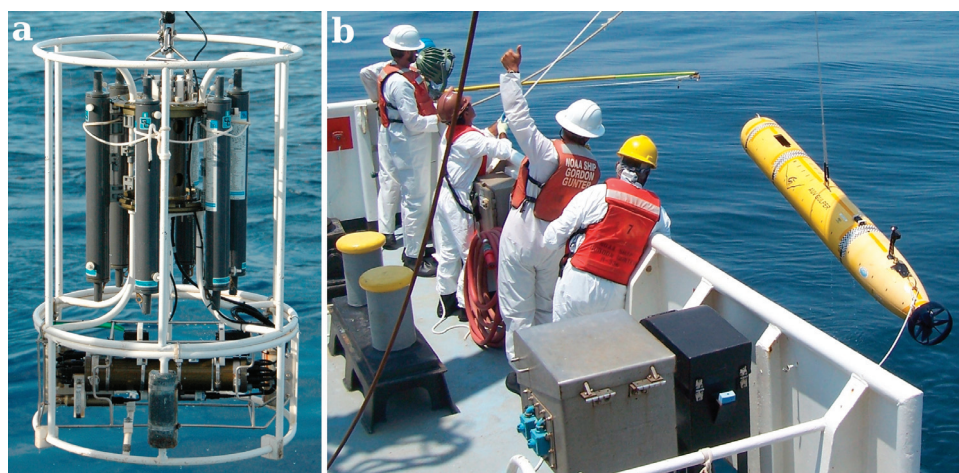


Figure 1. Deep-plume survey platforms used to collect data presented in this study. (a) Ship conductivity, temperature, and depth/colored dissolved organic matter (CDOM) rosette system. (b) The *Dorado* autonomous underwater vehicle (AUV), shown being recovered following a preliminary survey in the Gulf of Mexico.

Because our CDOM fluorometer was not calibrated specifically for the deep plume we observed, we present fluorometric signal from the CDOM fluorometer simply as F_{CDOM} , with the units of mg m^{-3} reflecting calibration according to the protocol of the instrument manufacturer [JAG, 2010b]. Following real-time examination of data profiles from the hydrocast sensors, focusing on F_{CDOM} signal that could indicate encounter with deep oil plumes, the depths for sampling were chosen to target signal peaks and background. Observed spatial variability in hydrocast F_{CDOM} was also the near-real-time data used to localize deep-plume signal for targeted deployment of the AUV.

2.2. AUV

The *Dorado* AUV is a robust platform for water column and seafloor research [Bellingham *et al.*, 2000; Sibenac *et al.*, 2002; Kirkwood, 2007]. Its modular design facilitates adaptability to observing needs, including support of specialized sensors and sampling systems [Bird *et al.*, 2007; Johnson and Needoba, 2008; Ryan *et al.*, 2010a; Maier *et al.*, 2011] and augmented power supply to enhance endurance. The *Dorado* platform mobilized for the Gulf of Mexico response (Figure 1b) was specialized for shallow pelagic ecology research. While the core vehicle is rated for operations to 6000 m depth, and its water samplers are rated for operations to 1500 m depth, not all components were sufficiently depth-rated for the response effort. In preparation for this effort, the vehicle's shallow-rated (1000 m) syntactic buoyancy foam was replaced with deep-rated foam, and four shallow-rated (300 m) sensors were removed. The shallow-rated sensor for measuring optical backscattering at two wavelengths and

chlorophyll fluorescence was replaced with a deep-rated equivalent. Finally, because CDOM fluorometers were adopted by the response community as a primary off-the-shelf optical sensor for detecting oil, a deep-rated CDOM fluorometer was added. Specifics of deployed sensors and their measurements are summarized in Table 1. To make

Table 1. Variables Measured With Sensors on the *Dorado* Autonomous Underwater Vehicle

Variable	Sensor
Temperature, salinity	Dual Sea-Bird Electronics SBE3 temperature and SBE4 conductivity sensors, using SBE25 conductivity, temperature, depth (CTD) board sets
Pressure	Paroscientific Digiquartz 8CB4000-I High Pressure Intelligent Depth Sensor, 0-4000 m range
Density	Derived from temperature, absolute salinity, and pressure [IOC <i>et al.</i> , 2010]
Dissolved oxygen concentration	Sea-Bird SBE43 oxygen sensor
Colored dissolved organic matter (CDOM) fluorescence	WET Labs ECO-FL CDOM fluorometer 370 nm excitation; 460 nm emission
Optical backscattering at 470 nm	HOBi Labs HydroScat-2
Optical backscattering at 676 nm	HOBi Labs HydroScat-2
Chlorophyll fluorescence at 676 nm (470 nm excitation)	HOBi Labs HydroScat-2

F_{CDOM} data from the AUV comparable with that from the ship hydrocast system, F_{CDOM} data from the AUV were adjusted. Cross-calibration employed data from the two ship hydrocast stations that had the strongest deep-plume signal, which were within the AUV survey domain, and data from AUV profiles nearest the ship hydrocast profiles and exhibiting similar vertical structure in F_{CDOM} signal. A linear least-squares regression was computed for the matchup data, and the AUV F_{CDOM} data were converted according to this relationship.

Prior to initial detection of deep-plume signal by the ship hydrocast system, *Dorado* test missions were periodically run in progressively deeper water, primarily to ensure that all systems were functional and to prepare for targeted mapping and sampling. This included acquisition of water samples with the AUV at prescribed depths. Following the first detection of deep hydrocarbon plume signal by the ship hydrocast system, which occurred late on 1 June through early 2 June, AUV missions were prepared to target the maximum signal localized by ship hydrocasts. Because deep-plume signals were first detected near the end of the cruise, with less than 48 h of available research

effort left, the remaining time was focused primarily on conducting high-resolution surveys and sampling with the AUV across the plume boundary and interior. A deep volume, centered on the maximum plume signal detected by ship hydrocasts, was surveyed using parallel vertical sections. The sections were oriented perpendicular to the vector between the wellhead and the survey location, with the intention of crossing the plume boundary at a series of distances from the blowout. Each vertical section was mapped using a sawtooth trajectory with six profiles between 900 and 1200 m. The deep boundary of the volume survey was constrained for safe operations above the local bathymetry. On 2 June, a brief (4 h) mission of two parallel vertical sections was completed. Data from this mission were used to finalize preparation of the algorithm for autonomous sampling of F_{CDOM} signal peaks [Zhang *et al.*, 2011], by modifying an algorithm previously used to sample plankton layers [Zhang *et al.*, 2010]. On 3 June, a longer duration (10 h) mission of seven parallel vertical sections was completed. AUV profile data had an average vertical resolution of 0.2 m; they were bin-averaged to 1 m resolution for analysis.

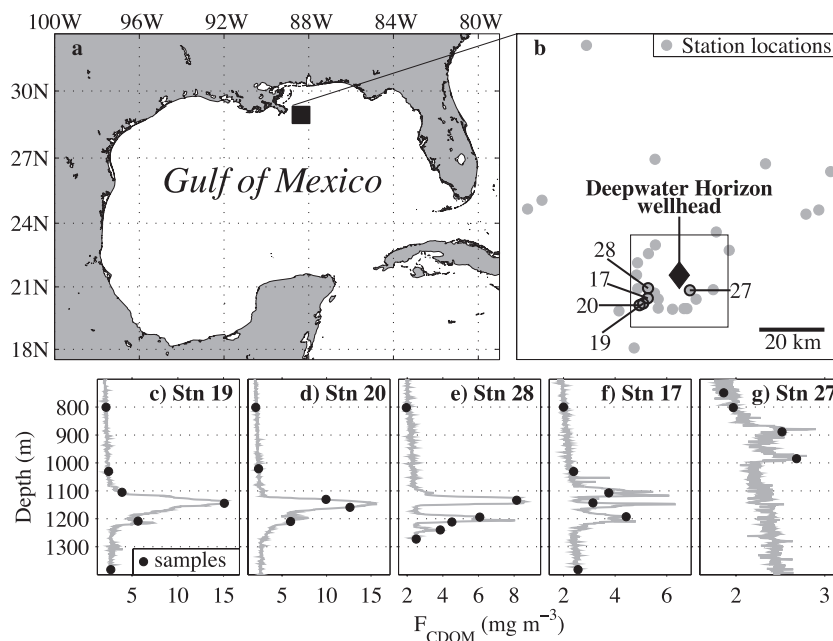


Figure 2. Summary of ship hydrocast station locations and optical data from deep-plume detection. (a) Location of the ship survey domain (black box). (b) Locations of all hydrocasts (gray) and those for which deep-plume optical signal was detected (black circles). The location of the *Deepwater Horizon* wellhead is 28.7396°N, 88.3668°W. Bathymetric detail of the inset box is shown in Figure 3. (c–g) Profiles of fluorescence signal measured by the CDOM fluorometer at the five stations for which deep-plume optical signal was detected. Profiles extended above and, in some cases, below the depth range shown. Black circles on the profiles indicate the locations of Niskin bottle samples. Station date-times are 17: 1 June 21:42, 19: 2 June 03:01, 20: 2 June 04:29, 27: 3 June 15:07, 28: 3 June 20:43.

2.3. Chemical Analysis of Samples

Sample handling, storage, transfer, and analysis followed the protocol established by NOAA. Samples were analyzed using Environmental Protection Agency standard methods that were modified by Alpha Lab for the set of petroleum hydrocarbons specified by NOAA. Specifically, Alpha Lab used methods 8015M (SOP. 0-003 Rev. 5), 8260M (SOP. 0-119 Rev. 2), and 8270M (SOP. 0-008 Rev. 6). Following analysis, results were compiled and provided by NOAA. In addition to concentrations, the chemical data included extensive metadata for evaluation of quantifiable results. Excluded from analysis were all reported concentration values below the reported detection limit and all results with quality codes indicating any of the following conditions: nondetect, unreliable results, tentative identification, or do-not-report (quality codes U, UJ, R, N, NJ, and DNR). Only reported concentrations passing the above criteria were used for examination of plume chemical composition and variability. Further, only results from stations at which F_{CDOM} indicated deep-plume signal are presented. For these stations, the concentration data were summed in three categories: (1) benzene, toluene, ethylbenzene, and xylenes (BTEX), (2) polycyclic aromatic hydrocarbons (PAHs), and (3) alkanes.

3. RESULTS

3.1. Ship Hydrocast Survey

The ship hydrocast survey encompassed a large area (Figure 2a) in search of subsurface oil. Although stations were occupied in all quadrants around the *Deepwater Horizon* wellhead, most were concentrated in a hemispherical arc centered southwest of the blowout (Figure 2b). The octagonal appearance of the station locations around this arc reflect Incident Command specification of an exclusion perimeter, using eight reference points that circumscribed a circle of 5 nmi in radius around the wellhead. Although this exclusion zone was in place for our operations during most of the cruise, its relaxation late in the cruise permitted some sampling slightly closer to the wellhead. Among the 30 stations, five profiles showed optical signal indicative of deep hydrocarbon plume encounter (Figures 2b–2g). Four of these were southwest of the blowout: stations 17, 19, 20, and 28. These were distinguished from station 27, southeast of the blowout, by optical signals that were both stronger and deeper (Figures 2b–2g). The two stations with the strongest optical signal (Figures 2c, 2d) had very similar profile structures dominated by a single peak, in contrast to multippeak structure evident in

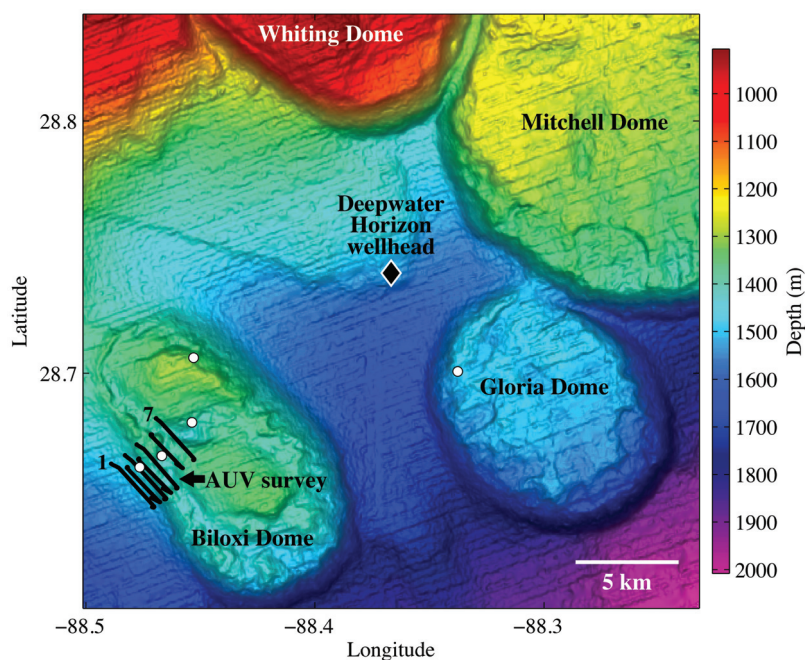


Figure 3. Ship and AUV deep-plume observation locations relative to bathymetry and the blowout source location. The domain shown is the inset box in Figure 2b. The AUV survey sections (black lines) were over the western flank of Biloxi Dome, centered on the hydrocast stations that exhibited the strongest deep-plume optical signal, stations 19 and 20 (Figure 2). Only the locations of the five hydrocast stations (white circles) exhibiting plume signal (Figure 2b) are shown.

the other profiles (Figures 2e–2g). Samples were acquired within all optical-signal peaks as well as in the optical-signal background around each peak (Figures 2c–2g).

3.2. AUV Survey

Localization of maximum deep-plume signal by the ship hydrocast survey (Figure 2) motivated the focus of AUV operations on a relatively small area over the western flank of Biloxi Dome (Figure 3). All AUV sections showed elevated F_{CDOM} within a deep plume, located toward the northern side of the survey domain, and all sections evidently crossed the southern boundary of the plume (Figure 4). In addition to the plume signal evident in F_{CDOM} , very similar signal was evident in optical properties measured by another sensor on the AUV. The similarity of these optical signals is evident in the interpolated vertical sections as nearly identical patterns of variation (Figure 4), and it is quantified by

examining relationships between F_{CDOM} and the other optical properties (Figures 5a–5c). F_{Chl} (Figure 5a) is fluorescence measured using wavelengths appropriate for the excitation of chlorophyll fluorescence and measurement of its emission (Table 1). This measurement, which is normally used as an imprecise proxy for phytoplankton abundance, detected bio-optical signal of phytoplankton chlorophyll in shallow waters (not presented). However, the F_{Chl} signal of the deep oil plume was much greater than the F_{Chl} signal of the shallow phytoplankton populations. The signal in optical backscattering (Figures 5b, 5c) is consistent with the dominance of particle scattering over absorption in the attenuation of light by this plume [Diercks *et al.*, 2010]. In addition to these optical measurements that covaried (Figures 5a–5c) and consistently defined deep-plume structure, oxygen measurements exhibited strong inverse variation with F_{CDOM} (Figure 5d). This signal is consistent with the biological oxygen demand of microbial degradation of hydrocarbons,

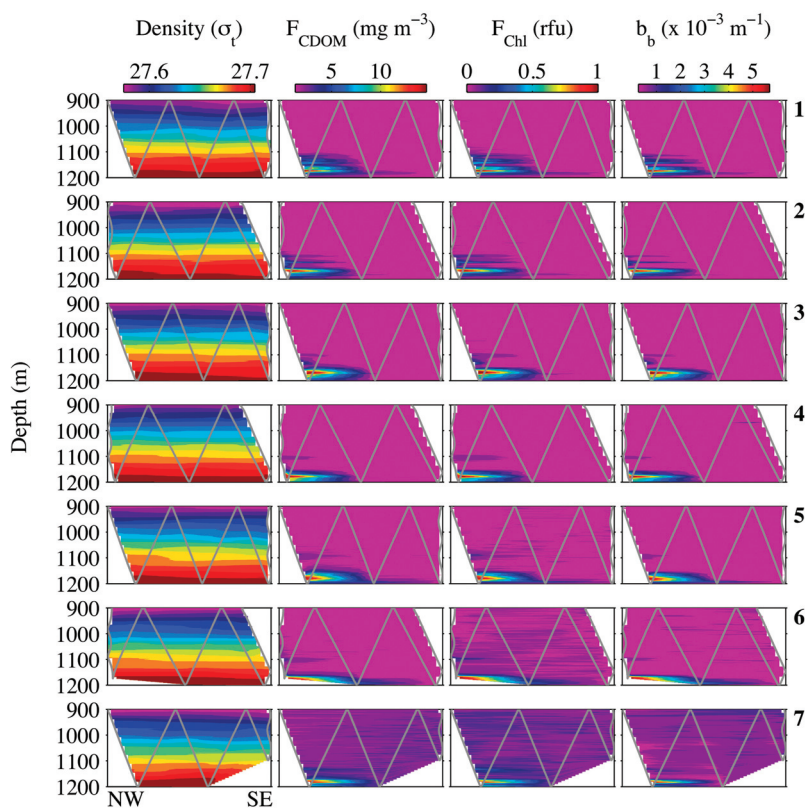


Figure 4. Interpolated properties mapped along the seven vertical sections of the 3 June survey (Figure 3). All sections are aligned such that the northwestern end is to the left. The gray lines show the AUV trajectory through each section. F_{CDOM} is fluorometric signal from the CDOM fluorometer, cross-calibrated with that from the CDOM fluorometer on the ship hydrocast system. F_{Chl} is uncalibrated fluorescence from the chlorophyll fluorometer (Table 1); rfu, relative fluorescence units, normalized relative to the maximum value measured; b_b , optical backscattering at 470 nm.

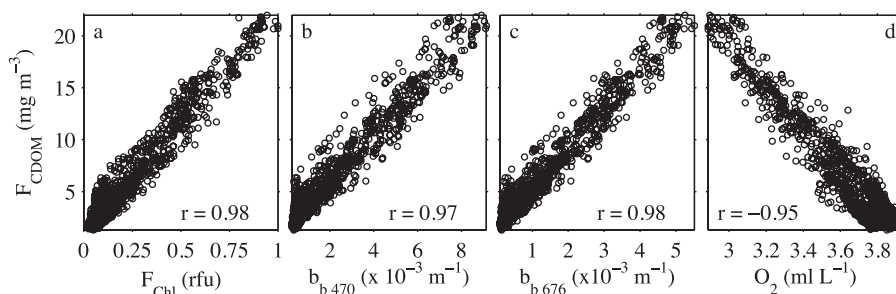


Figure 5. Scatterplots of AUV F_{CDOM} versus the four other AUV sensor readings that exhibited signal from the deep plume. Correlation coefficients are noted.

and oxygen drawdown was indicated by analysis of oxygen data in this plume [JAG, 2010d; Valentine *et al.*, 2010; Kessler *et al.*, 2011].

To objectively define the plume and describe its structure within the area surveyed by *Dorado*, it was necessary to distinguish plume optical signal from natural background signal. Maximum F_{CDOM} exhibited a linear increase between 200 and 1000 m (Figure 6), and this was used as the basis to define a depth-dependent maximum expected background F_{CDOM} . Extrapolation of this linear relationship through the depth range 1000 to 1200 m defined the maximum expected background across the depth range of interest, and plume signal intensity was quantified as F_{CDOM} above the maximum expected background. Apply-

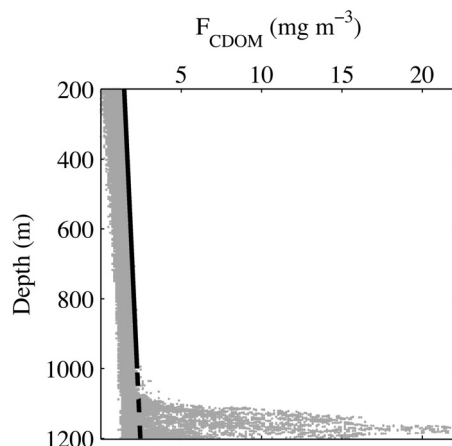


Figure 6. Definition of plume relative to background. Points show all AUV F_{CDOM} data acquired from the plume surveys of 2–3 June. The solid line shows the linear fit between maximum F_{CDOM} and depth for the depth range 200 to 1000 m, and the dashed line shows the extrapolation of this linear relationship between 1000 and 1200 m. Plume signal is defined as F_{CDOM} above the depth-dependent maximum expected background value.

ing this quantification of plume intensity and linear interpolation between the vertical sections (Figure 4) permitted description of the synoptic structure of the plume boundary and interior (Figure 7).

A contour map of maximum plume intensity measured in each of the 42 AUV profiles indicates a close small-scale relationship between bathymetry and plume structure. Specifically, the maximum plume intensity was found along the upper slope of Biloxi Dome, and the plume core was evidently aligned with the dome's slope-top break (Figure 7b). Further, while isopleths of plume intensity were oriented approximately perpendicular to dome-slope isobaths, they were oriented approximately parallel to dome-top isobaths (Figure 7b). These patterns are consistent with southeastward flow of the plume core along the western slope of Biloxi Dome and spreading of the plume onto the dome top. At intermediate levels of intensity between the outer boundary of the plume (Figure 7c) and its most intense core (Figure 7f), the plume layer reached shallower depths over the dome slope than over its top (Figures 7d, 7e).

3.3. Plume Chemical Composition

The software developed to autonomously recognize plume optical-signal peaks and sample them with the AUV worked as planned during the 3 June survey. The design and results of this algorithm can be found in the work of Zhang *et al.* [2011]. Although the software functioned effectively, the signals it sent to trigger AUV samples were blocked by a flooded controller housing. Therefore, our examination of plume chemical composition is based entirely on analysis of samples returned by the ship hydrocast system. Further, the presentation of sample analysis data is constrained to the five stations that exhibited optical signal from the deep plume (Figure 2). Control samples above and below deep-plume optical signal, as well as from profiles exhibiting no deep-plume optical signal, were examined to verify

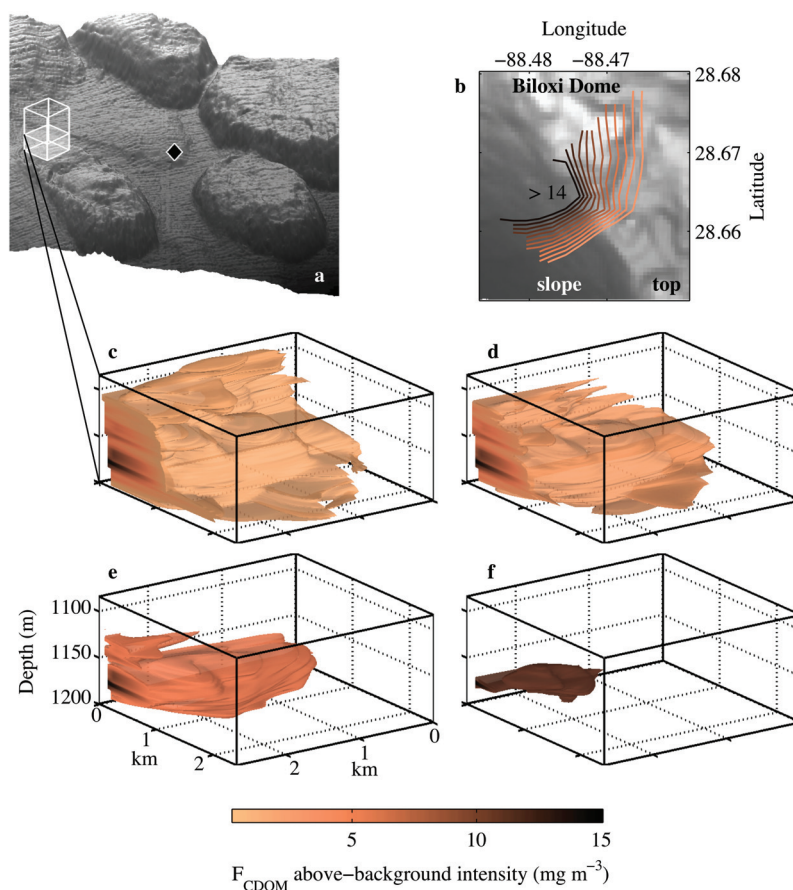


Figure 7. High-resolution structure of the deep plume, based on the definition of background (Figure 6) and interpolation between the AUV sections (Figure 4). (a) AUV survey domain relative to 3-D topographic map (as in Figure 3). (b) Contours of F_{CDOM} plume signal, based on the maximum signal detected in each of the 42 profiles (Figure 4). (c–f) Volume views of the deep plume at a series of increasing levels of intensity, beginning with the boundary at which F_{CDOM} exceeded the maximum expected background (Figure 6). Each volume view represents the highlighted subdomain of the full AUV survey volume shown in (a). The interpolated model is based on more than 65,000 F_{CDOM} measurements within the 900–1200 m depth range acquired in less than 10 h.

comparatively negligible levels of quantifiable hydrocarbons. However, we do not present any results from non-plume samples.

For samples acquired from the deep plume southwest of the wellhead (Figures 2c–2f), the relative proportions of major chemical groups were similar, with BTEX the most abundant, followed by alkanes and PAHs (Figures 8a–8c; Table 2). The dominance of BTEX in this plume was also noted in a separate study of its composition [Reddy *et al.*, 2011]. The composition of the weaker deep plume sampled southeast of the wellhead (Figures 2b, 2g) exhibited greater disproportion in the relative abundance of BTEX (Figure 8d; Table 2). At the two stations within the AUV survey domain, samples from the near-peak optical signal showed that concentrations of 117 individual hydrocarbon compounds were

nearly equal over a range of concentrations that spanned more than four orders of magnitude (not shown).

Measurement of F_{CDOM} by an off-the-shelf optical sensor, as was widely used in the scientific response, served as an effective proxy for chemical concentrations in the plume that we surveyed. As much as 97% (median 88%) of the variance in the concentrations of individual chemical compounds could be predicted from a linear relationship with F_{CDOM} (e.g., Figure 9a). For most chemical compounds, the linear relationship with F_{CDOM} could explain >80% of the variance in concentration (Figure 9b). Variation in F_{CDOM} also explained a large proportion of the variance in total chemical concentrations within the categories of total extractable matter, BTEX, alkanes, and PAHs (Figure 9b), ranging from 90% for alkanes to 63% for BTEX.

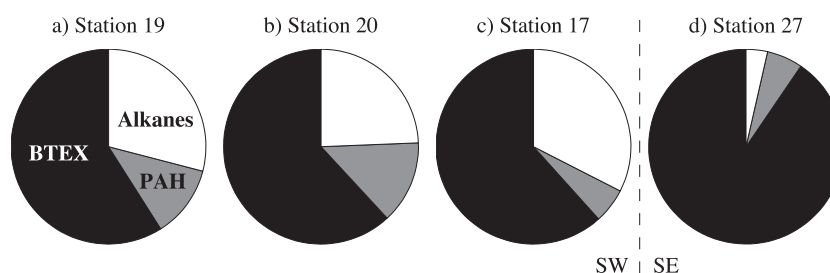


Figure 8. Description of deep-plume chemical composition in terms of the proportions of total chemical concentrations in each of three major groups, BTEX, alkanes, and PAHs. Corresponding concentration data and percentages are presented in Table 2. The results are from samples having the highest total extractable matter in each of the hydrocasts showing deep-plume optical signal (Figure 2). Station 28 is not shown because no sample for volatile organic analysis was acquired at that station (Table 2).

4. DISCUSSION

When destruction of the *Deepwater Horizon* drilling rig caused complete loss of control over the wellhead 1500 m below the surface, the potential for severe pollution to spread over great distances arose in a major environmental crisis. The required management and mitigation efforts were monumental, and the need for accurate information and effective solutions drew from a spectrum of existing and emergent technologies. Remotely operated vehicles from the industrial and scientific sectors converged on the damaged wellhead with intensive efforts to understand and solve the problem at its source. A variety of existing and emergent technologies were applied to mitigate harm at the surface. While effort at the ocean boundaries was a natural focus, understanding the transport and effects of pollution within the vast volume between the boundaries was also important. Although the formation of deep plumes of dispersed oil was a known possible consequence of blowout fluid dynamics, deep-plume formation during the Macondo blowout was likely enhanced by the application of chemical dispersants [JAG, 2010c; Socolofsky *et al.*, 2011]. Formation of this deep pollutant pool occurred where its observation was challenging and its removal was infeasible. Rapidly adapted technol-

ogies played a key role in understanding its nature and potential consequences.

Interpretation of deep-plume signal was complicated by a number of factors, including potential hydrocarbon signal from natural seafloor seeps and delay in the provision of analysis results from plume chemistry samples, caused by sample processing backlogs and development of the data management and reporting system. However, by the time the first summary report was released by the Joint Analysis Group on 20 June 2010, without chemical analysis results, the preponderance of evidence indicated that oil existed in the deep water column southwest of the blowout, and multiple observations indicated that the source of this deep plume was the blowout [JAG, 2010a]. These observations included (1) the plume's origin at the damaged wellhead, (2) its extension southwest of the blowout in agreement with deep current patterns, (3) its decreasing intensity with distance from the wellhead, and (4) vertical separation of the deep plume and the local seafloor away from the blowout, indicating a layer with a nonlocal source across the region of its extension. Also at this early stage, the JAG concluded that a deep plume would be expected due to effects of dispersion at the wellhead. The second summary report released on 20 July 2010 provided additional data indicating the persistence

Table 2. Categorized Total Hydrocarbon Concentrations, in $\mu\text{g L}^{-1}$ and (Corresponding Percentages of the Total) for the Sample Having the Highest Total Extractable Matter in Each Hydrocast That Showed Deep-Plume Optical Signal (Figure 2)^a

Station	BTEX	Alkanes	Polycyclic Aromatic Hydrocarbons
20	262.0 (62%)	103.2 (24%)	58.1 (14%)
19	234.3 (59%)	115.3 (29%)	47.5 (12%)
28	NA ^a	45.3	23.4
17	62.4 (62%)	32.9 (32%)	5.9 (6%)
27	50.5 (90%)	2.0 (4%)	3.3 (6%)

^aNA indicates no VOA sample was collected.

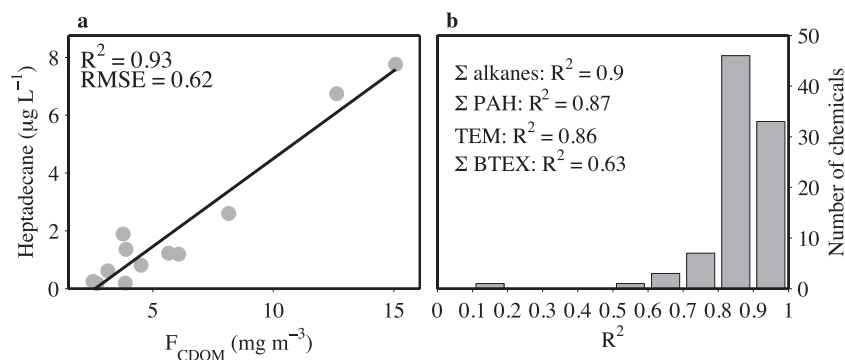


Figure 9. Off-the-shelf optical measurements as a chemical proxy, evaluated using all matchups from ship hydrocast sampling (Figures 2c–2g). (a) Example of scatterplot, linear relationship, and statistics of the linear relationship between F_{CDOM} and an individual chemical compound. (b) Histogram of the coefficient of determination (R^2) between F_{CDOM} and all individual hydrocarbon compounds quantified from hydrocast samples. The R^2 values for the relationships between F_{CDOM} and summed concentrations within categories are noted; TEM, total extractable matter. Corresponding correlation coefficients for all categories are significant at $p < 0.001$.

of a plume southwest of the blowout [JAG, 2010b]. Further studies of the same data set [Diercks *et al.*, 2010; Hazen *et al.*, 2010] and additional survey data [Valentine *et al.*, 2010] also supported the link to the blowout and began to examine the microbial dynamics relevant to biological degradation of hydrocarbons.

Although analysis of the ship hydrocast optical data made a convincing case for the source of the plume, a more definitive link between the deep plume and the blowout came from data acquired by the rapidly adapted *Sentry* AUV [Camilli *et al.*, 2010]. Using results from an in situ mass spectrometer and concurrent measurements of deep current velocity, the researchers quantified the input rate of monoaromatic petroleum hydrocarbons to the plume and showed that this rate far exceeded the input rate possible from all northern Gulf seafloor seeps combined. Our ship hydrocast and AUV observations approximately 3 weeks before the *Sentry* operations did not have sufficient coverage or resolution to definitively link the plume to the blowout. In fact, our hydrocast survey found maximum plume signal in an area where natural seafloor seeps were concentrated [JAG, 2010a; Figure 46]. However, the plume attributes described by our data are very consistent with results from surveys of the Macondo deep plume made by six other ships [JAG, 2010a, 2010b; Diercks *et al.*, 2010; Hazen *et al.*, 2010; Valentine *et al.*, 2010] as well as the *Sentry* AUV [Camilli *et al.*, 2010]. Additionally, remotely operated vehicle (ROV) video only 0.5 km southwest of the blowout, acquired the same day our first hydrocast detected deep-plume signal approximately 10 km southwest of the blowout, showed that the depth range over which we detected deep-plume F_{CDOM} signal was very similar to the vertical distribution of a dis-

persed oil plume recorded by ROV video [Camilli *et al.*, 2010]. Starting only 1 week after our AUV survey, a ship survey revealed a deep plume of dissolved hydrocarbon gasses from the blowout and associated oxygen depletion in the same depth range and area that we found the maximum optical and chemical signals, along the western side of Biloxi Dome [Valentine *et al.*, 2010]. Also similar to our findings, they mapped a weaker plume southeast of the wellhead between ~ 750 and 1000 m. Based on the consistency of our observations with all Macondo blowout deep-plume observations southwest of the wellhead acquired during May and June, we conclude that our AUV survey mapped a portion of a plume from the Macondo blowout, not a natural seafloor seep.

Bathymetric steering of currents along the continental slope was a factor noted by observational and modeling studies of the deep oil plume extending southwest of the blowout [JAG, 2010a; Liu *et al.*, 2011, this volume]. The synoptic plume survey conducted with the *Sentry* AUV during the blowout period [Camilli *et al.*, 2010] and the large-scale ship survey conducted after the well was sealed [Kessler *et al.*, 2011] provided the clearest depictions of this relationship. In addition to this bathymetric influence on plume transport over scales of tens to hundreds of kilometers, influence of bathymetry on flow at smaller scales was indicated by the exceptionally high-resolution mapping of a plume boundary zone by the *Dorado* AUV. Based on the synoptic patterns of plume intensity and gradients, we interpret that we surveyed a plume filament extending southeastward along the western slope of Biloxi Dome. We observed very close alignment between the plume-filament's most intense core and the dome's slope-top break. Further, a

change in the orientation of plume gradients relative to isobaths was observed across the dome slope-top break. The orientation of plume-filament isopleths approximately perpendicular to dome-slope isobaths is consistent with along-isobath transport from the north. The orientation of plume isopleths approximately parallel to dome-top isobaths is consistent with flow from the dome-slope, where its intensity was greatest, up onto the dome top, where its intensity was weaker. We interpret that our hydrocast survey simply did not have sufficient spatial resolution or coverage to resolve the main plume, which was known to extend at least 10 km southwest of the wellhead by 25 May [JAG, 2010a]. Instead, our hydrocast survey localized a small region within which detailed structure of a plume filament was observed.

Because AUV profiles consistently sampled the peak intensity and shallow boundary of the plume, small-scale spatial variation in these plume parameters can be examined reliably relative to bathymetry. Small-scale spatial variation in other important parameters, including plume thickness and the height of the plume's bottom boundary relative to bathymetry, could not be robustly examined due to limitations in the data. Constrained to a maximum depth of 1200 m, the AUV profiles did not consistently sample the bottom boundary of the plume (defined as F_{CDOM} falling below background at the deep boundary). This limitation in the AUV data is consistent with the ship profile data in the same region, which showed the bottom boundary of the plume between ~1225 and 1275 m. The two ship CTD profiles in the region of the AUV plume survey were too sparse to define spatial variation. Despite these limitations, the high-resolution AUV survey, targeted using ship hydrocast data, uniquely described the apparent steering of plume lateral transport by a small-scale bathymetric feature.

With our optical and chemical data of the deep plume, we examined how well a simple optical measurement from an off-the-shelf sensor served as a proxy for concentrations of a variety of chemical compounds. This limited analysis is relevant to interpreting the optical description of the deep plume that we mapped with ship and AUV systems. Within this data set, collected over a relatively small spatial and temporal scale, we found that a simple optical measurement served as an effective proxy for individual chemical compounds as well as total concentrations of chemicals in specific categories (alkanes, PAHs, BTEX). Our findings are consistent with those of Wade *et al.* [this volume] who report an R^2 of 0.80 for the relationship between total PAH concentrations and fluorescence in their data set, which was collected during a period overlapping with our study. Analysis of much larger combined data sets that are now available is needed to evaluate spatial and temporal variation in the

relationships between optical and chemical signals of subsurface plumes.

Because major scientific challenges arose suddenly from this disaster, the response was indeed a record-breaking enterprise in terms of mobilization of scientific resources, adaptation of technology, and integration of results. With short time for mobilization, targeting, and deployment, the *Dorado* AUV proved to be an effective tool for studying a difficult-to-observe process of pollutant transport. Readiness for this urgent deployment was primarily due to the similarity between the requirements of mapping and sampling deep oil plumes and the requirements of studying complex natural coastal ocean phenomena, the purpose to which *Dorado* is routinely applied. Data from an off-the-shelf optical sensor supported mapping of the plume boundary zone and interior structure and provided a reasonably accurate description of quantitative variation in hydrocarbon concentrations. Plume signal was detected clearly in five of the eight measurements made by *Dorado*, suggesting the potential for combinations of low-cost off-the-shelf sensors to disambiguate dispersed oil from natural CDOM. Improvements to the plume-detection algorithm applied in the Gulf can better optimize targeted sample acquisition [Zhang *et al.*, 2011]. The sampler controller housing that flooded on the final day of operations had withstood dives to 1200 m the previous day. Its potential failure was a known risk that simply could not be mitigated on the short time scale of mobilization to the Gulf; however, this risk would be readily mitigated by modifying the pressure-compensating mechanism of the housing. Additionally, augmented AUV capabilities are motivated by this incident, particularly by the considerable spatial scale of the deep plume and the complexity of its dispersion and degradation. These improvements include greater endurance [e.g., Bellingham *et al.*, 2010], more capable onboard autonomy for tracking evolving plumes [e.g., Farrell *et al.*, 2005; Camilli *et al.*, 2010], and optimization of sensing and sampling capabilities.

Acknowledgments. This work was supported by the David and Lucile Packard Foundation and NOAA Sea Grant under grant CFDA 11.473/RCOOS S673. We thank J. Bellingham, S. Etchemendy, and C. Scholin (MBARI) for leading the mobilization of *Dorado* to the Gulf of Mexico; D. Conlin, D. Thompson, G. Massion, D. French, and M. Conway (MBARI) for help preparing the AUV for mobilization; and C. Scholin for valuable suggestions on AUV data analysis. R. Brown (NOAA) served as the Chief Scientist of cruise GU-10-02, and the able assistance of the *Gordon Gunter* crew was greatly appreciated. The CDOM fluorometer for the hydrocast system was provided by A. Remsen. CTD hydrocasts conducted by G. Zapfe (NOAA) and ship-borne EK60 echo sounder profiles processed by T. Weber and S. Greenaway (University of New Hampshire) informed AUV deployment plans. R. McEwen

and J. Bellingham (MBARI) and C. Thompson (NOAA) contributed to the development of the AUV's peak-capture algorithm. Z. Willis, S. Walker, B. Shorr, J. Farr, and J. Brinkman (NOAA) were instrumental in providing and reviewing the results of chemical analyses. D. Caress and M. McCann (MBARI) provided the Gulf of Mexico bathymetry data shown in Figure 3, and M. McCann ensured postprocessed AUV navigation was accurate for the UTM zone of the Gulf surveys. D. Rutz (NOAA) provided accurate latitude and longitude for the *Deepwater Horizon* wellhead.

REFERENCES

- Bellingham, J. G., K. Streitlien, J. Overland, S. Rajan, P. Stein, J. Stannard, W. Kirkwood, and D. Yoerger (2000), An Arctic basin observational capability using AUVs, *Oceanography*, 13, 64–71.
- Bellingham, J. G., et al. (2010), Efficient propulsion for the *Tethys* long-range autonomous underwater vehicle, paper presented at Autonomous Underwater Vehicles 2010, Oceanic Eng. Soc., Monterey, Calif.
- Bird, L. E., A. D. Sherman, and J. P. Ryan (2007), Development of an active, large volume, discrete seawater sampler for autonomous underwater vehicles, paper presented at MTS/IEEE Oceans 2007, Mar. Technol. Soc., Vancouver, B. C., Canada.
- Camilli, R., C. M. Reddy, D. R. Yoerger, B. A. S. Van Mooy, M. V. Jakuba, J. C. Kinsey, C. P. McIntyre, S. P. Sylva, and J. V. Maloney (2010), Tracking hydrocarbon plume transport and biodegradation at *Deepwater Horizon*, *Science*, 330(6001), 201–204, doi:10.1126/science.1195223.
- Diercks, A.-R., et al. (2010), Characterization of subsurface polycyclic aromatic hydrocarbons at the *Deepwater Horizon* site, *Geophys. Res. Lett.*, 37, L20602, doi:10.1029/2010GL045046.
- Farrell, J. A., S. Pang, and W. Li (2005), Chemical plume tracing via an autonomous underwater vehicle, *IEEE J. Oceanic Eng.*, 30, 428–442.
- Hazen, T. C., et al. (2010), Deep-sea oil plume enriches indigenous oil-degrading bacteria, *Science*, 330(6601), 204–208, doi:10.1126/science.1195979.
- IOC, SCOR, and IAPSO (2010), The international thermodynamic equation of seawater—2010: Calculation and use of thermodynamic properties, *Intergovernmental Oceanographic Commission, Manuals and Guides 56*, 196 pp., UNESCO, Paris, France.
- Joint Analysis Group (JAG) (2010a), Review of R/V *Brooks McCall* data to examine subsurface oil, report, NOAA, Silver Spring, Md. [Available at <http://www.ncddc.noaa.gov/activities/healthy-oceans/jag/reports/>.]
- Joint Analysis Group (JAG) (2010b), Review of preliminary data to examine subsurface oil in the vicinity of MC 252 #1, May 19 to June 19, report, NOAA, Silver Spring, Md. [Available at <http://www.ncddc.noaa.gov/activities/healthy-oceans/jag/reports/>.]
- Joint Analysis Group (JAG) (2010c), Initial quality control of analytical chemistry data from water samples taken in the vicinity of MC 252#1, report, NOAA, Silver Spring, Md. [Available at <http://www.ncddc.noaa.gov/activities/healthy-oceans/jag/reports/>.]
- Joint Analysis Group (JAG) (2010d), Review of preliminary data to examine oxygen levels in the vicinity of MC 252 #1, May 8 to August 9, report, NOAA, Silver Spring, Md. [Available at <http://www.ncddc.noaa.gov/activities/healthy-oceans/jag/reports/>.]
- Johnson, K. S., and J. A. Needoba (2008), Mapping the spatial variability of plankton metabolism using nitrate and oxygen sensors on an autonomous underwater vehicle, *Limnol. Oceanogr.*, 53, 2237–2250.
- Kessler, J. D., et al. (2011), A persistent oxygen anomaly reveals the fate of spilled methane in the deep Gulf of Mexico, *Science*, 331(6015), 312–315, doi:10.1126/science.1199697.
- Kirkwood, W. J. (2007), Development of the *Dorado* mapping vehicle for multibeam, subbottom, and sidescan science missions, *J. Field Robotics*, 24(6), 487–495.
- Liu, Y., R. H. Weisberg, C. Hu, and L. Zheng (2011), Tracking the *Deepwater Horizon* oil spill: A modeling perspective, *Eos Trans. AGU*, 92(6), 45, doi:10.1029/2011EO060001.
- Liu, Y., R. H. Weisberg, C. Hu, and L. Zheng (2011), Trajectory forecast as a rapid response to the *Deepwater Horizon* oil spill, in *Monitoring and Modeling the Deepwater Horizon Oil Spill: A Record-Breaking Enterprise*, *Geophys. Monogr. Ser.*, doi:10.1029/2011GM001121, this volume.
- Maier, K. L., A. Fildani, C. K. Paull, S. A. Graham, T. R. McHargue, D. W. Caress, and M. McGann (2011), Evolution of deep-marine channels from high-resolution AUV surveys offshore ntral California, *Geology*, 39, 327–330, doi:10.1130/G31589.1.
- Reddy, C. M., et al. (2011), Composition and fate of gas and oil released to the water column during the *Deepwater Horizon* oil spill, *Proc. Natl. Acad. Sci. U. S. A.*, doi:10.1073/pnas.1101242108.
- Ryan, J. P., J. F. R. Gower, S. A. King, W. P. Bissett, A. M. Fischer, R. M. Kudela, Z. Kolber, F. Mazzillo, E. V. Rienecker, and F. P. Chavez (2008a), A coastal ocean extreme bloom incubator, *Geophys. Res. Lett.*, 35, L12602, doi:10.1029/2008GL034081.
- Ryan, J. P., M. A. McManus, J. D. Paduan, and F. P. Chavez (2008b), Phytoplankton thin layers within coastal upwelling system fronts, *Mar. Ecol. Prog. Ser.*, 354, 21–34.
- Ryan, J. P., A. M. Fischer, R. M. Kudela, J. F. R. Gower, S. A. King, R. Marin III, and F. P. Chavez (2009), Influences of upwelling and downwelling winds on red tide bloom dynamics in Monterey Bay, California, *Cont. Shelf Res.*, 29, 785–795.
- Ryan, J. P., S. B. Johnson, A. Sherman, K. Rajan, F. Py, H. Thomas, J. B. J. Harvey, L. Bird, J. D. Paduan, and R. C. Vrijenhoek (2010a), Mobile autonomous process sampling within coastal ocean observing systems, *Limnol. Oceanogr. Methods*, 8, 394–402.
- Ryan, J. P., M. A. McManus, and J. M. Sullivan (2010b), Interacting physical, chemical, and biological forcing of phytoplankton thin-layer variability in Monterey Bay, California, *Cont. Shelf Res.*, 30, 7–16.
- Ryan, J. P., A. M. Fischer, R. M. Kudela, M. A. McManus, J. S. Myers, J. D. Paduan, C. M. Ruhsam, C. B. Woodson, and Y. Zhang (2010c), Recurrent frontal slicks of a coastal ocean upwelling shadow, *J. Geophys. Res.*, 115, C12070, doi:10.1029/2010JC006398.

- Schrope, M. (2010), *Deepwater Horizon: A scientist at the center of the spill*, *Nature*, 466, 680–684, doi:10.1038/466680a.
- Sibenac, M., W. J. Kirkwood, R. McEwen, F. Shane, R. Henthorn, D. Gashler, and H. Thomas (2002), Modular AUV for routine deep water science operations, paper presented at Oceans 2002 Marine Frontiers, Mar. Technol. Soc, Biloxi, Miss.
- Socolofsky, S. A., E. E. Adams, and C. R. Sherwood (2011), Formation dynamics of subsurface hydrocarbon intrusions following the *Deepwater Horizon* blowout, *Geophys. Res. Lett.*, 38, L09602, doi:10.1029/2011GL047174.
- Valentine, D. L., et al. (2010), Propane respiration jump-starts microbial response to deep oil spill, *Science*, 330, 208–211, doi:10.1126/science.1196830.
- Wade, T. L., et al. (2011), Analyses of water samples from the *Deepwater Horizon* oil spill: Documentation of the subsurface plume, in *Monitoring and Modeling the Deepwater Horizon Oil Spill: A Record-Breaking Enterprise*, *Geophys. Monogr. Ser.*, doi:10.1029/2011GM001103, this volume.
- Zhang, Y., R. S. McEwen, J. P. Ryan, and J. G. Bellingham (2010), Design and tests of an adaptive triggering method for capturing peak samples in a thin phytoplankton layer by an autonomous underwater vehicle, *IEEE J. Oceanic Eng.*, 35, 785–796, doi:10.1109/JOE.2010.2081031.
- Zhang, Y., R. S. McEwen, J. P. Ryan, J. G. Bellingham, H. Thomas, C. H. Thompson, and E. Rienecker (2011), A peak-capture algorithm used on an autonomous underwater vehicle in the 2010 Gulf of Mexico oil spill response scientific survey, *J. Field Robotics*, 28, 484–496, doi:10.1002/rob.20399.
-
- S. R. Cummings, NOAA Atlantic Oceanographic and Meteorological Laboratory, Miami, FL 33149, USA.
- R. K. Nelson, Woods Hole Oceanographic Institution, Woods Hole, MA 02543, USA.
- E. V. Rienecker, J. P. Ryan, H. Thomas, and Y. Zhang, Monterey Bay Aquarium Research Institute, 7700 Sandholdt Rd., Moss Landing, CA 95039-9644, USA. (ryjo@mbari.org)

